Non-contact measurement of the temperature profile of PET preforms.

Bortolino Saggin, Marco Tarabini, Diego Scaccabarozzi, Luca Cornolti[1], Hermes Giberti[2], Giovanni Moschioni.

Politecnico di Milano, Dipartimento di Meccanica, Lecco Campus, Via Previati 1/C, 23900 Lecco

Abstract

This paper describes a system for the measurement of the internal and external temperature profiles of PET preforms used in the Injection Stretch Blow Moulding (ISBM) process. Many works in literature highlighted the importance of these quantities to improve the production quality of PET bottles, but none addressed the development of a measuring system suitable for this scope. A measuring system based on two thermopiles for the identification of the internal temperature profile and a thermal camera for the measurement of the external one has been designed. The adopted sensors were individually calibrated and the uncertainty budget, accounting for both instrumental uncertainties and the effect of multiple reflections, was derived. A prototype of the measuring system was tested on an industrial ISBM machine. The dependence of the preforms temperature profile on the settings of the ISBM machine was investigated. Results evidenced that the minimum variations of the machine settings induced temperature differences significantly larger than the measurement uncertainty, thus proving the effectiveness of the proposed system.

1 Introduction

In recent years, the need of lowering the costs and the environmental impact of plastic bottles production has brought to a continuous reduction of the quantity of material used to produce each specimen. This process is not straightforward, as the reduction of the bottles' thickness increases the risk of production wastes.

The most employed technology to produce polyethylene terephthalate (PET) bottles (1) is based on two stages. In the first one, a thick compact polymer preform is produced through a classical injection

---

[1] Now with SUPSI.

[2] Now with University of Pavia.

moulding process. In the second stage, called injection stretch blow moulding (ISBM), the preform follows a complex process. At first it is sent into an infrared (IR) oven where it is heated above the glass transition temperature of PET. The heated preform is then transferred into a mould, where it is stretched by a rod and blown with compressed air until it assumes the bottle shape. The quality of the product (absence of shape defects and top-load strength properties) requires a proper distribution of the material of the preform over the whole surface of the mould.

The dynamics of the stretch-blow phase is strongly affected by the visco-plastic properties of PET, which are in turn dependent on the temperature (2). Experiments and numerical simulations have shown that the optimal performance of the stretch-blow phase is achieved when the temperature of the preform is neither homogeneous nor monotonic (3) (4) (5). The optimal temperature distribution is achieved by controlling the amount of energy irradiated by different layers of IR lamps constituting the oven, and by tuning the time delay between the exit from the oven and the stretch moulding phase. The heating process of the preform is influenced by too many variables to allow for the usage of fixed power ovens (5). Moreover, factors such as the environmental temperature or the preform thermo-optical and geometrical properties or the production rate may change, and the ISBM machine must be able compensate their effects. Consequently, the setting of the process parameters (as for instance the lamps power distribution) requires tuning whenever the type of product changes and sometimes also during the ordinary operation of an ISBM machine. Nowadays, experienced technicians , with a try and error process, find the acceptable operating conditions. A more effective approach would implement an automatic feedback control system allowing to obtain the desired temperature profile on the preform by regulating power of the oven lamps. This system would minimize the wastes, the machine downtime, and would allow for additional material saving on the single bottle by operating the ISBM process always with the optimal temperature profile. The first step to implement the process automation is the development of a system preforming the temperature profile measurement providing the feedback signal required for a closed loop control system. This system should be included in the production line and should allow detecting the temperature on both the internal and external surfaces of the preform. The last requirement depends on the low thermal conductivity of PET (6) and on the heating process which allows for non-negligible thermal gradients across the preform thickness.

This work presents the design and validation of a measurement system matching the above requirements for the ISBM machine temperature profile automatic control. The proposed system is based on infrared (IR) detectors, extensively used in industrial applications (7) (8) (9) and also . The working temperature range in ISBM is between 75°C and 130°C, which are respectively the glass transition and crystallization temperatures limits (10). PET behaves like an opaque body in the wavelength range between 6 and 14 μm (6) (11), and consequently IR sensors working in this spectral range allow measuring the surface temperature. The simultaneous use of two sensors allows evaluating the global difference across the thickness of the preform: IR cameras were used in previous works to detect the temperature of the external surface of the preform (6) (11). Nevertheless, the measurement uncertainty has never been

addressed despite it is crucial for the feasibility of a control loop, it will be therefore a significant part of this work. Moreover, previous works dealt only with the external preform temperature measurement and were mainly focused on the evaluation of the effect of the temperature on the stretch-blow phase (12) (13) and the validation of numerical models (5) (11) (14) .

2 Measuring Instruments and method

2.1 Instruments

The non-contact temperature measurements were performed using an infrared camera NEC TH7102WX (spectral range 8-14 μm) and the thermopiles General Electric ZTP-115 (spectral range 6-14 μm). The thermopiles were selected because of their small size in addition to their metrological characteristics, fully matching the requirements of our application. The thermal camera type (i.e. micro-bolometric detector 320x240 pixels (14)) is nowadays the workhorse in IR mapping, besides the specific instrument was used in previous measurements on plastic materials (15) and fully characterized also from a dynamic point of view (16).

In our setup, the IR camera is used to map the temperature of the external surface of the preform and two thermopiles are mounted on a support (Figure 1.a) which slides inside the preform. The motion is provided by a linear motor controlled by an Arduino DC motor driver board (17). One of the thermopiles is scanning the lateral surface of the preform, while the other one is axially mounted and allows probing the preform bottom. Figure 7.b shows the entire setup; the thermal camera was located in the position from which this picture was taken.

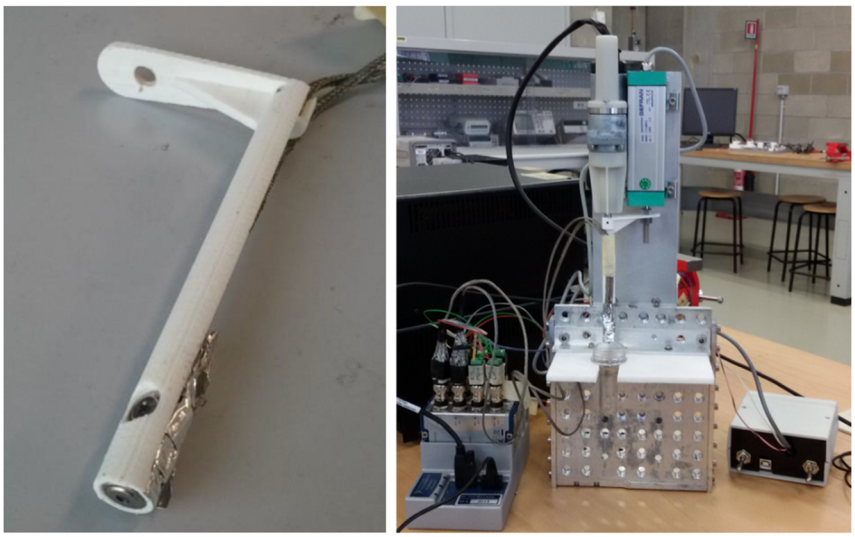

***Figure 1**. Setup design: a) thermopiles support. b) Overall setup.*

The prototype measures the temperature of a preform taken out from the ISBM machine, but the system has been conceived to be eventually mounted directly on line. The PET preform selected as reference for the system validation is the one for the transparent (pigment free) 0.5 litre bottle. Its geometrical

features are presented in Figure 2. Since the emissivity of PET is influenced by various factors such as the degree of crystallinity (18), (10) the production procedure and the geometry of the preform, the actual material composition, therefore it is important to measure its emissivity. The emissivity of preforms of various shapes and colours have been preliminarily measured, in order to assess the possibility of using a fixed value of emissivity for each lot or even for any PET preform.

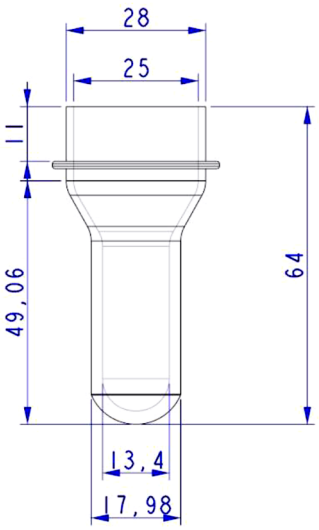

***Figure 2**. Preform geometry*

2.2 Preform emissivity characterization

The IR camera was used to measure the preforms emissivity. The actual preform temperature was measured by a Platinum resistance thermometer, as shown in the scheme of Figure 3.

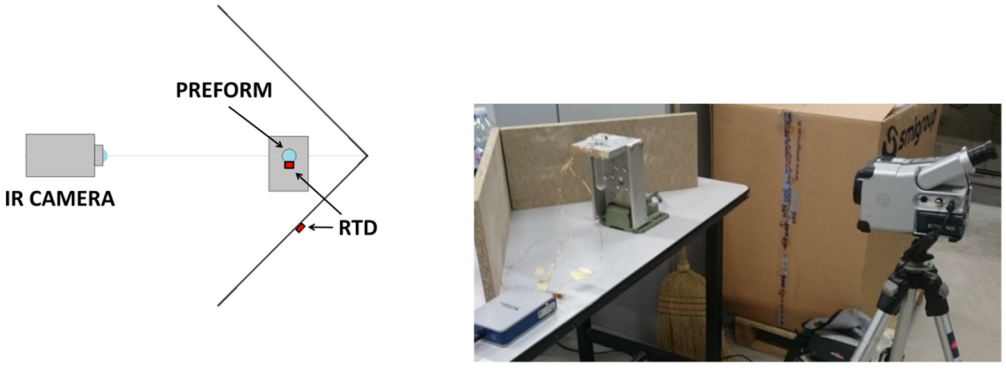

***Figure 3**. Setup for the estimation of the emissivity of PET preform: a) scheme of the experimental system. b) Picture of the setup.*

The output of the infrared camera (T_{out}), corresponds to that of a Black Body (BB) having the same radiosity of the source. Starting from Stephan-Boltzmann equation (20), the relationship that correlates

the incoming radiance (w_{net}) with the indicated temperature (T_{out}) and the temperature of the object (T_o) is:

$$w_{net} = \sigma T_{out}^4 = \sigma \varepsilon_o T_o^4 + \sigma(1 - \varepsilon_o) T_b^4 \quad (1)$$

Where ε_o, T_o are respectively the emissivity and temperature of the investigated object. $\rho = 1 - \varepsilon_o$ is the reflectivity of the observed body assuming that its transmissivity is negligible (11); T_b is the background temperature and σ is the Stephan-Boltzmann constant. Despite the adopted instruments are working in the 8 ÷14 μm or 6 ÷14 μm bands, the Stefan-Boltzmann equation can still be used because the fraction of power in these bands is constant (within a 1% error) for emitters in the temperature range from 20 to 100 °C. This means that the band limitation can be included in the window transmittance, that can still be considered constant with respect to the source temperature; besides, this assumption has been verified experimentally with the thermopiles calibration as will be seen in the following Eq. 1 can therefore be rearranged to compute the object emissivity:

$$\varepsilon_o = \frac{T_{out}^4 - T_b^4}{T_o^4 - T_b^4} \quad (2)$$

In our tests, the preforms were heated to about 70°C, T_o and T_b were measured with Pt100 RTDs mounted respectively on the preform and the panels surrounding the specimen (see Figure 3). The emissivity of the external surface was measured on four samples of each preform lot to assess the property spread.

2.3 Thermopile calibration.

In the thermopile, the sensing element is the hot junction of a series of thermocouples, whose cold junction temperature is that of the detector case. The latter is typically measured by an internal thermistor. In steady conditions, the incoming power, W_{net} is directly proportional to the temperature difference between the thermopile junctions, that in turns is directly proportional to the output voltage V (21). Eventually one can write:

$$V = S\, W_{net} = S\sigma A_s F \tau_w \left(\varepsilon_o T_o^4 + (1 - \varepsilon_o) T_b^4 - T_s^4\right) \quad (3)$$

T_s is the sensor temperature, S is the sensor sensitivity and A_s is the sensor area. F is the view factor between the sensing area and the source, τ_w the sensor window transmittance and ε_o the source emissivity (unitary when calibrating with a black body), T_b the background temperature T_o the source temperature. Eq. 3 can be re-arranged to highlight a global calibration constant, connecting the output voltage with the difference of the fourth power of temperatures during calibration with a black body source.

In our tests, the temperature of the blackbody was measured with a Pt100 RTD and the thermopile output voltage was recorded. The calibration constant was evaluated through a least square linear fitting (22) of the input-output data. The calibration constant C was made non-dimensional (Eq. 4) by including the known sensors parameters i.e. the nominal sensitivity S and the area A_s. Equation (3) becomes:

$$\Delta V = C\, SA_s\sigma(T_o^4 - T_s^4) \tag{4}$$

Since the measurement of the preform surface temperature requires a relative motion between the thermopile and the preform, the sensor dynamic behaviour was relevant too. The dynamic calibration was performed using the step input response: a shutter was interposed between a source at fixed temperature and the detector. Since the thermopile behaves like a first order instrument (20), the step input response was used to determine its time constant. According to the model the expected response to the step input is in the form: $V(t) = V_2 - (V_2 - V_1)e^{-t/\tau}$ (5)

2.4 Uncertainty

The instrumental uncertainty of the infrared camera was evaluated in a previous work through repeatability tests (16). The repeatability was evaluated from the analysis of 300 frames of a black body. The determined standard deviation on each pixel of the frame, $u(T_{out})$ follows a saddle distribution (minimax) over each frame and is 0.2°C for the pixels near the edges of the array. The bias error was negligible in the range 0-100 °C in comparison to the repeatability. The uncertainty of temperature measurements nevertheless, has to account also for the uncertainty of the object's emissivity. Using the ISO-GUM (23) approach, the uncertainty of the object temperature $u(T_o)$ is given by:

$$u(T_o) = \sqrt{\left(\frac{\partial T_0}{\partial T_{out}}u(T_{out})\right)^2 + \left(\frac{\partial T_0}{\partial \varepsilon_o}u(\varepsilon_o)\right)^2 + \left(\frac{\partial T_0}{\partial T_b}u(T_b)\right)^2} \tag{6}$$

$u(\varepsilon_o)$ is the uncertainty of the preform emissivity. The same procedure was applied also to the thermopiles measurements; Eq. 3 can be written as:

$$T_0 = \sqrt[4]{\frac{1}{\varepsilon_o}\left[\frac{V}{CA_sS\sigma} + T_s^4 - (1-\varepsilon_o)T_b^4\right]} \tag{7}$$

The uncertainty of the object temperature associated with the thermopiles $u(T_{o,p})$ can be evaluated as:

$$u(T_{o,p}) = \sqrt{\left(\frac{\partial T_0}{\partial \varepsilon_0}u(\varepsilon_0)\right)^2 + \left(\frac{\partial T_0}{\partial V}u(V)\right)^2 + \left(\frac{\partial T_0}{\partial C}u(C)\right)^2 + \left(\frac{\partial T_0}{\partial T_s}u(T_s)\right)^2 + \left(\frac{\partial T_0}{\partial T_b}u(T_b)\right)^2} \tag{8}$$

The uncertainty on the calibration constant $u(C)$ was estimated from the LS linear fitting. The standard deviation of measurements performed in repeatability condition was used to quantify the uncertainty of the output voltage $u(V)$, being this quantity larger than the uncertainty of the acquisition board (declared by the manufacturer).

Finally, the temperature of the sensor T_s was measured with the thermistor of the thermopile. In this case, the measurement uncertainty $u(T_s)$ included the contribution of the reading circuit.

Concerning the background temperature, the situation is quite different for the camera and thermopile measurements. The camera measures the outer temperature in an environment mostly at ambient temperature; the sensitivity coefficient to background temperature in Eq. (8) contains the $(1-\varepsilon_o)\,T_b^3$ term, that is small in comparison with the others because of the high emissivity, close to 0.9 and of a T_b much lower than T_{out}. The thermopile conversely, measures the inner temperature and the background is mostly due to the neighbouring surfaces of the preform; moreover, the background temperature changes with the measurement point (given that the sensor slides inside the preform, whose temperature profile is not constant). T_b is actually a compact way of writing the average contribution of the various parts of the background, and in general it can be written as:

$$T_b = \sqrt[4]{\frac{\sum_{j=1}^{N} R_{s,j} T_j^4}{\sum_{j=1}^{N} R_{s,j}}} \tag{9}$$

Where N is the number of isothermal portion of the background, $R_{s,j}$ is the radiative exchange factor of the detector (REF) with the j-th portion of the background whose temperature is T_j. In our case, two main background components at a temperature significantly different than the preform ones, have been identified, i.e. the ambient and the detector. The latter becomes significant with the small enclosure area generated inside the preform, so because of the reflections the detector has a REF with itself, this is the so-called narcissus effect. The sensors holding structure was eventually fully coated with a vacuum deposited aluminium tape having emissivity lower than 5% at the purpose of making its temperature non-significant. The REFs values have been computed using a Monte Carlo raytracing program, modelling the preform and thermopiles holder geometry and considering the position of the latter on a grid of 10 mm depths, to inspect different conditions during the temperature profile measurement. **Figure 4** shows how the narcissus and the ambient contribute to the background at various distances of the sensor axis from the preform border at a distance equal to zero (when the detector is just entering in the preform) about 50% of the REF is with the environment, so the temperature measurement is not significant.

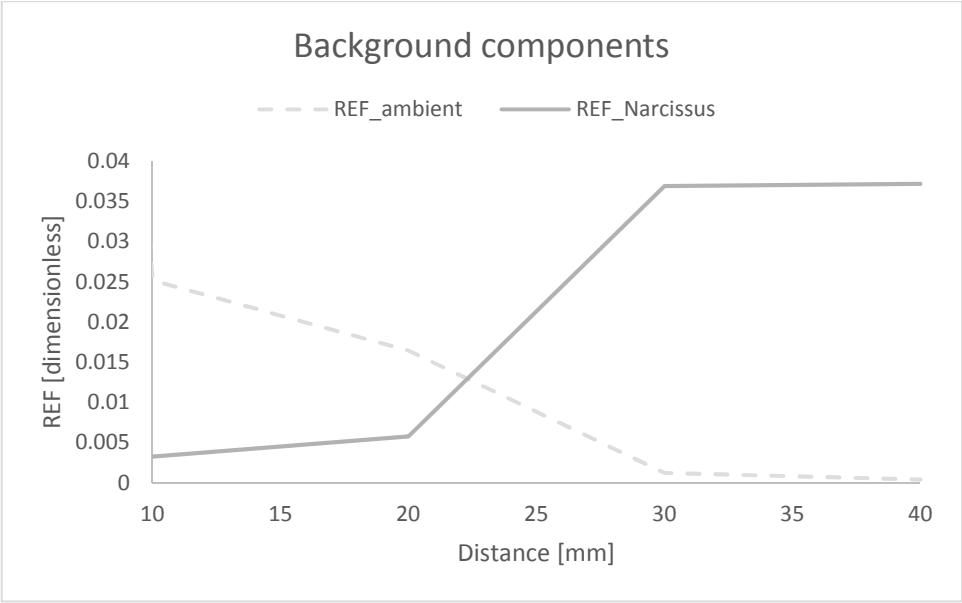

Figure 4 *Radiative Exchange Factors (REF) of backgrounds components for thermopile measuring the lateral temperature profile at various distances from the preform border*

At distances between 10 mm (i.e. where the measurements have been actually used) and 30 mm the effect is decreasing from 2.5 % to 0.1%. The contribution due to the reflections from other parts of the cavity is almost constant close to 10% . T_b uncertainty has been therefore evaluated considering equation (9), as combined uncertainty deriving from the REF variability at the various measuring positions and the temperatures uncertainties.

3 Measurements on the ISBM machine

The system described in the previous section was tested on an industrial ISBM machine manufactured by SMIgroup (24). The temperature profile of preforms leaving the infrared oven was measured with different machine configurations. The investigated parameters were selected among those that influence the heating process and can be controlled by the operator; these parameters were the intensity of the IR lamps and the production rate that determines the speed within the oven.

Both parameters were initially set to the average values for standard production condition and were afterwards modified by applying the minimal change that, according to the operator's experience, should induce a detectable effect on the bottles' quality. Table 1 shows the list of conditions characterizing the various tests. The lamps intensity was reduced by 5% with respect to the nominal value, referred to as "standard"; the decrease of the same amount was applied to the different layers of the IR lamps of the oven (see Figure 5.b). The line speed was reduced by 10% with respect to the standard condition to simulate a small change of the production rate. As can be seen in Table 1, the power of IR lamps of layer A was always kept at the standard value (i.e. maximum) as, according to the operator experience, the region near the ring was already close to the minimum in the test conditions.

	Condition 1	Condition 2	Condition 3	Condition 4	Condition 5	Condition 6

Power of lamps layer A	Standard	Standard	Standard	Standard	Standard	Standard
Power of lamps layers B and C	Standard	-5%	Standard	Standard	-5%	Standard
Power of lamps layers D and E	Standard	Standard	-5%	Standard	Standard	-5%
Production velocity	Standard	Standard	Standard	-10%	-10%	-10%

Table 1. *List of tests performed on the ISBM machine. To relate the lamp layers name with their positions in the oven, see Figure 5.b.*

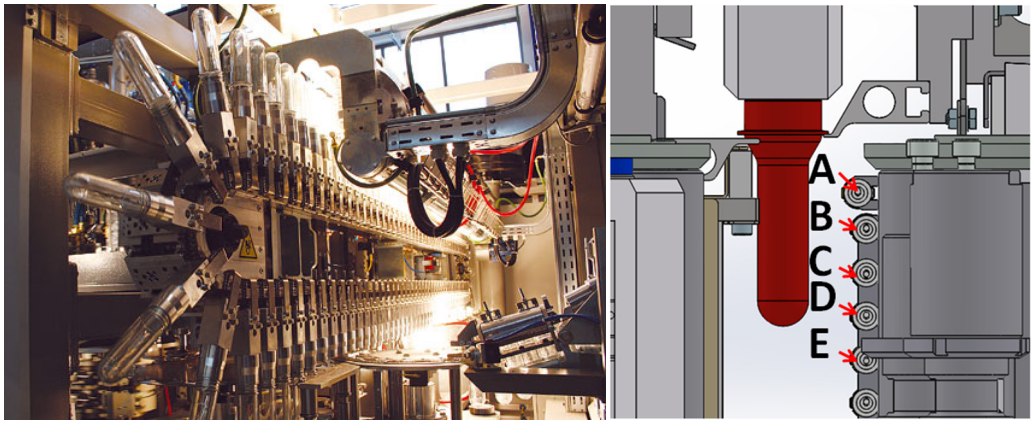

Figure 5. *a) Heating module of the ISBM machine employed in this work. b) Disposition of the infrared oven lamp layers.*

The test methodology was chosen in order to replicate the usual procedure of machine parameters tuning. After the selection of the parameters, the machine was run for five minutes without loading preforms to let the system stabilize. Three repetitions were performed in each configuration; the machine was turned off for about 10 minutes between the repetitions. The infrared camera was set to record five frames per second; its spatial resolution was about 0.6 mm per pixel. The time evolution of the temperature obtained from the camera was analysed to determine the cooling rate of the preform.

The temperatures measured by the thermal camera were statistically analysed on the region shown in Figure 6; the area was 76 x 5 pixels in size. The maximum variation observed within the same row was 0.25°C. The temperature profile along the vertical line is similar to the one obtained by the thermopile.

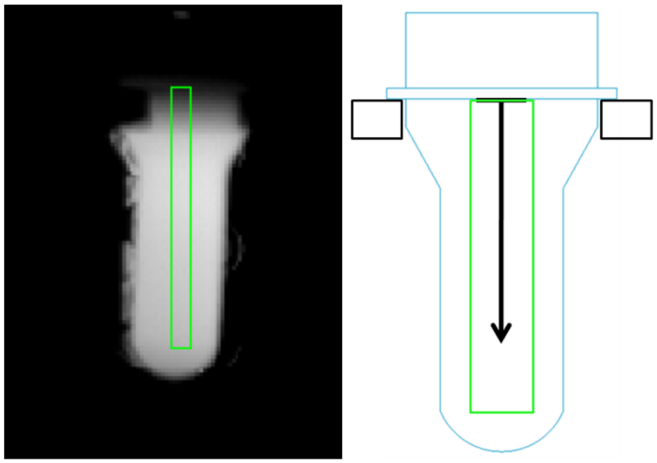

***Figure 6**. Example of image taken from the IR camera: on the left the investigated region is shown. On the right the same region is presented on sketch of the preform.*

4 Measurements results

4.1 Preforms emissivity

The measured emissivity of the external surface of the reference preform samples are shown in Table 2, together with the standard uncertainty.

	External Surface	
Preform number	**Emissivity**	**Standard Uncertainty**
1	0.872	0.008
2	0.861	0.008
3	0.870	0.008
4	0.889	0.008

***Table 2**. Emissivity of the external surfaces of the tested preforms and related measurement uncertainty.*

The average emissivity of the external surface is 0.873 with a standard deviation of 0.012. This value is larger than the measurement repeatability (0.008), so differences between the emissivity of preforms belonging to the same lot is inferred.

Four different types of preforms, with different colours, underwent this procedure; for each colour, four samples were analysed. The overall average emissivity of the external surface is 0.878, very close to the value identified for the transparent type. The overall measurements standard deviation is 0.031, more than twice the one observed on the single lot, evidencing differences between the different types.

4.2 Thermopiles characterization

The results of the static and dynamic calibration of the thermopiles are shown in Figure 7 a and b, which correspond to the models of Eq. 3 and 5. The good agreement (linearity SD below 1% of full scale) in both cases confirms that these models are representative of the actual behaviour of the thermopiles. The calibration process led to the calibration constant $C = 0.4977 \pm 0.0007$ and time constant 7.8 ± 0.2 ms.

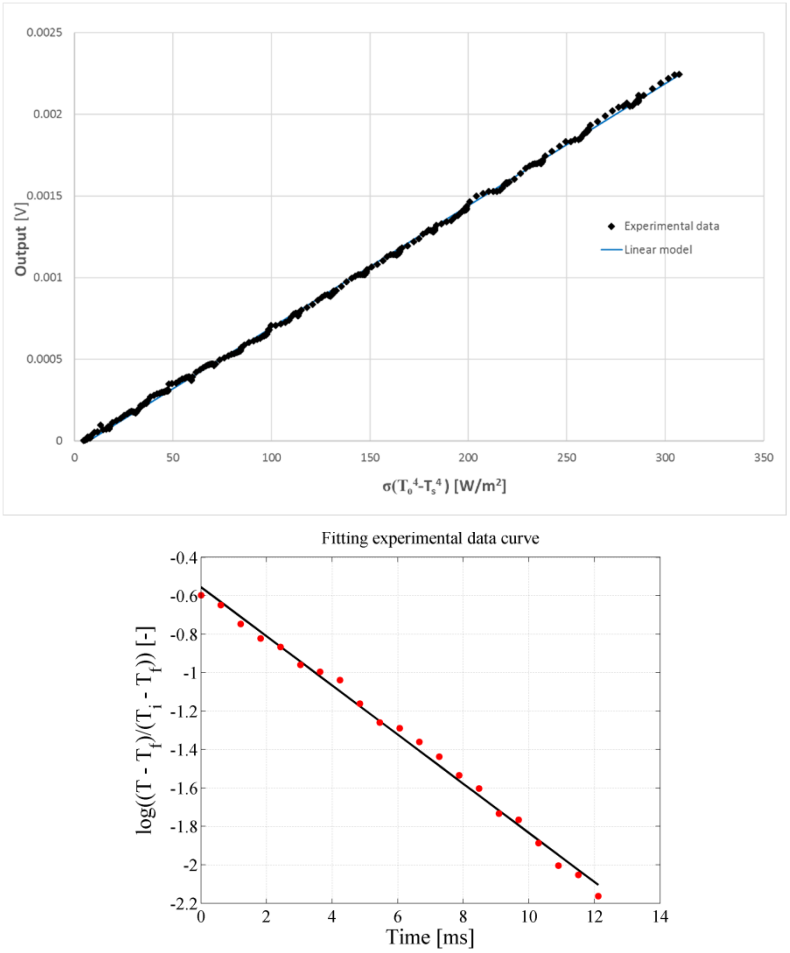

***Figure** 7. Calibration of the thermopile: upper plot: comparison of the LS fitting curve (Eq. 4) and the experimental data. Lower plot: estimation of the time constant (comparison between the LS linear fitting curve of the first order model and the experimental data).*

4.3 Uncertainty budget

Figure 8 shows the dependence of the temperature measurement uncertainty on the temperature itself, for both the IR camera (Eq. 6) and the thermopiles (Eq. 8). The uncertainties of the parameters used for the computations are summarized in Table 3.

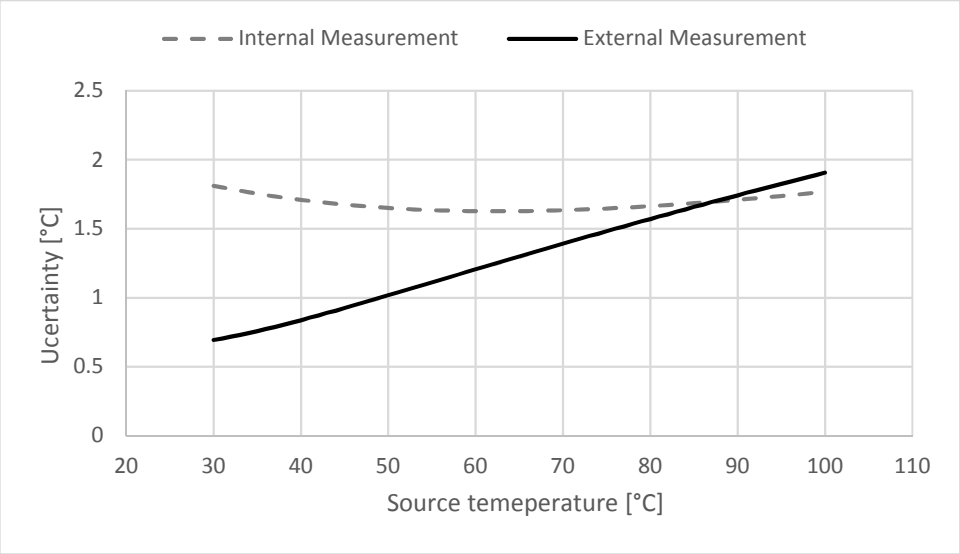

Figure 8. *IR camera and thermopile expanded uncertainty LC 95%, as function of the investigated object temperature (Eq. 6 and Eq. 8).*

Quantity	**Standard Uncertainty**	**Evaluation method**
$u(\varepsilon_0)$	0.012 [-]	Sample standard deviation.
$u(\Delta V)$	0.029 mV	Noise standard deviation.
$u(C)$	0.0007 [-]	Standard deviation of the parameter, from LS estimation
$u(T_s)$	0.4°C (maximum value in the range 20-40°C)	ISO GUM Type B evaluation
$u(T_b)$	1 °C (for eq.6) 2.6 °C (for eq.8)	Background temp. standard deviation
$u(T_{out})$	0.2 °C	Standard deviation from Thermal Imager calibration.

***Table 3**. Uncertainties used in Eq. (6) and (8) to evaluate the uncertainty related to the object temperature.*

For the external temperature measurement, the main source of uncertainty is the emissivity therefore the uncertainty is almost proportional to the temperature as it would be if the emissivity would be the only uncertainty source. For the internal temperature measurement, the voltage uncertainty of thermopiles is prevailing at low temperatures, but the effect decreases as the temperature of the source increases: as a result, the total uncertainty decreases at higher temperatures. The uncertainties of the two measurements are comparable in the temperature range of interest, but the external measurement is dominated by the emissivity contribution while in the internal one it is reduced because of the cavity effect.

The breakdown of the uncertainty budget allows understanding whether it is necessary to identify the emissivity of each preform before the non-contact measurement or not. At 100°C the uncertainty using the average emissivity of the preform type is about 2 °C; in the ideal case of the perfect knowledge of the preform emissivity ($u(\varepsilon_0) = 0$), this value would decrease to 0.56°C. With the use of an average emissivity for all the type of preforms, the uncertainty at 100°C would be 2.6°C for the thermopiles and 4.8°C for the camera. Using an average emissivity value would lead to a bias error on the temperature measurements while the system is processing the same lot of material. The control system using this measurement to tune the lamps power in order to maintain the reference temperature profile would generate an equivalent bias error of a few degrees; this is considered still acceptable for a correct process.

4.4 Preform temperature distribution

Figure 9 shows the measured temperatures of the external surface of the preform for conditions 1, 2, 3 and 4. The plot shows the temperature profiles (average of the three tests repetitions) in order to highlight the effects of the machine parameters. The data dispersion between the tests repetitions is highlighted by the dashed lines. The temperature repeatability in nominally identical tests does not allow recognizing the effect of the change in the power of the layer D-E of the IR lamps. Conversely, the change in the power of layers B-C is well evidenced.

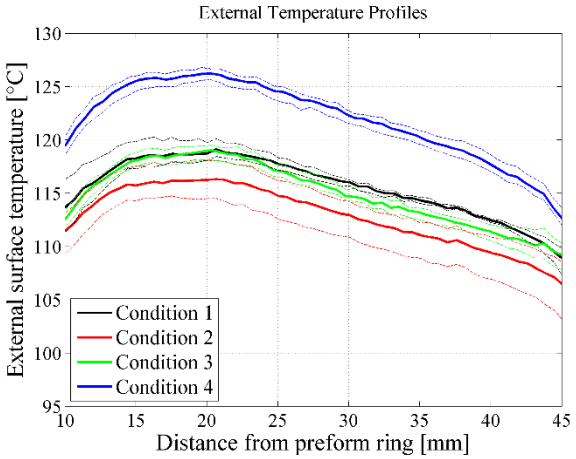

***Figure 9**. Temperature profiles for conditions 1, 2, 3 and 4, dotted lines evidence the repeatability standard deviation.*

Figure 10 compares the average of internal and external temperature profiles. As the setup was designed to investigate the zone near the neck of the preform, which is the region where the differences between the external and internal temperatures are higher, only the 10 mm closest to the ring are reported.

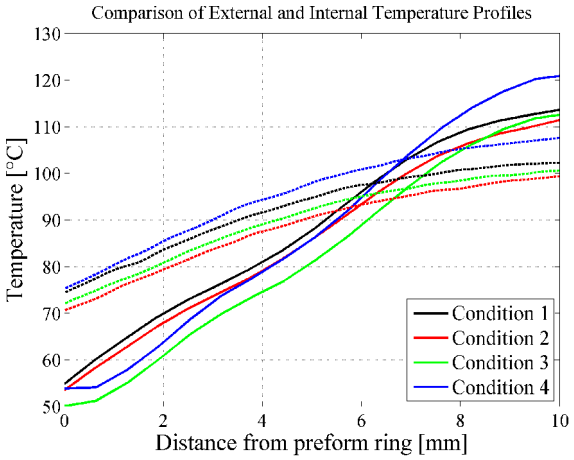

***Figure 10**. Comparison of the averaged temperatures profile of the inner and outer surfaces for conditions 1, 2, 3 and 4; solid lines represent the external profiles, dotted lines the internal.*

Figure 11 shows the evolution of the temperatures with time for the heating condition 1. The temperature was measured at four positions at increasing distance from the preform ring, highlighted in the scheme in figure 10. This allows evidencing the variation of the preforms thermal profile and determining the temperature drop from the IR oven exit to the measurement start.

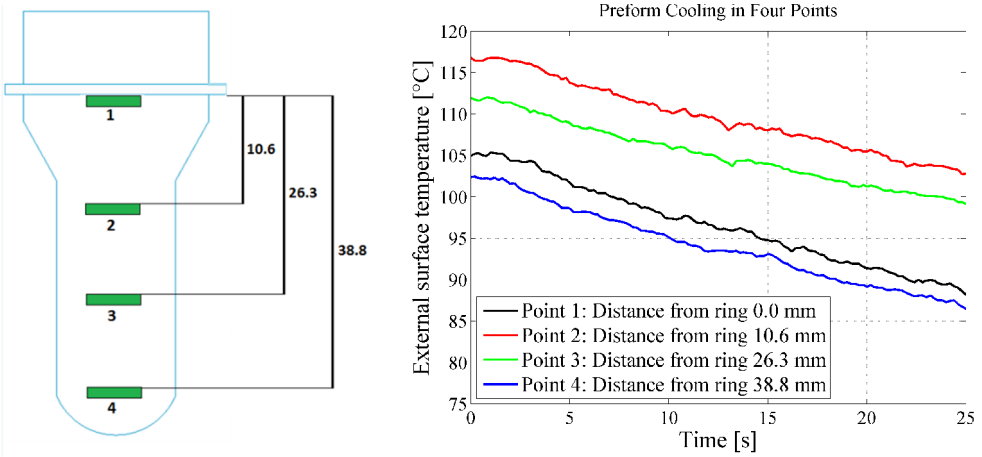

***Figure 11**. Temperature time evolution for four points of the preform: a) Position of the considered points. b) Temperature history of the four points.*

5 Discussion

The effectiveness of the proposed measurement system was evaluated by assessing the setup capability to detect the effect of minimal variations of machine settings. The discrimination threshold required to the system has been identified at first, then, the metrological performances of the measurement system have been compared with it.

5.1 ISBM Heating Process

The measurements presented in the previous section show that the temperature profiles are very similar to those considered ideal at the purpose of achieving a correct material distribution during the ISBM (3). The region close to the preform ring (neck region) is well below the glass transition temperature (75°C); then the temperature rapidly increases reaching temperatures between 115°C and 120°C at a distance of 10 mm below the neck. Ideally, the PET below the ring should behave like a viscous material and should exhibit low resistance to deformation: the zone above the neck should not be deformed at all to keep the correct shape of the bottle cap. PET property changes along the preform length are obtained through a temperature gradient in this region. Starting from the hottest part, after a short plateau of about 10 mm, the temperature slowly decreases and in the last 30 mm the temperature is approximately 10°C lower than the maximum value.

In our tests, the parameter mostly affecting the temperature is the reduction of the production rate. The decrease of production rate by 10% (i.e. a longer staying inside the IR oven) increased the temperature profile of about 9°C along all the preform. The reduction of the lamps intensities induces a minimal temperature reduction with respect to the standard condition. In particular, conditions 1 and 3 are very close, with a difference of about 1°C in the zone between 20 and 40 mm. In configuration 2, this deviation increases to 2-3°C, in agreement with the lamps arrangement. The results for conditions 5 and 6 (not reported in this work) are very close to condition 4, confirming the predominant effect of the production rate. The temperatures measured in our tests sometimes rose above 125°C; of these preforms exhibited crystallization after some minutes of cooling in air.

The temperature differences of the internal surface measured in different machine configurations are coherent with those observed on the external surface. The effect of the decreased production rate was smaller than that noticed on the external surface, given that the maximum temperature difference decreased from 10 °C of condition 1 to 6°C in condition 4. The comparison of temperatures on the internal and external surfaces of the preform shows that the inner temperature is always higher than the outer one in the region close to the ring of the preform, while after 6 mm the temperature gradient is reversed.

The proposed measurement system allowed detecting the cooling rate of the heated preforms; the cooling rate of four different areas is approximately the same. Consequently, the preform temperature

distribution does not become uniform during the travel between the oven and the moulding module. In all the tests, the estimated preform cooling rate in still air is close to 0.4 °C/s. The repeatability of the procedure was assessed by the sample standard deviation for the first four conditions; results are summarized in Table 4.

Condition	Maximum Standard deviation [°C]	Average Standard deviation [°C]
1	0.9	0.4
2	2.2	1.9
3	0.8	0.6
4	2.5	2.2

***Table 4**. Sample standard deviation for the first 4 tested conditions of table 1. The reported values are related to the maximum and spatial average in the range between 20 and 40 mm.*

The manual extraction procedure took a variable time estimated between 2 and 4 seconds, which could induce a temperature change between 1 and 2 °C. Consequently, the standard deviation related to conditions 2 and 4 reasonably depends on this cause of uncertainty. Moreover, as the employed machine setting identification number follows the run time order, the results suggest that there is no time dependence of the measurements standard deviation.

5.2 Measurement System

The uncertainty budget shows that the proposed system is not suitable to detect temperature differences smaller than 1°C. This implies that the machine settings 1 and 3 cannot be clearly discriminated, given that the temperature differences are comparable with the measurement uncertainty. The difference between settings 1 and 3 was a 5% reduction of the power of lamps D and E. As the position of these lamps (Figure 5) is below the preform, only a small fraction of their radiation is absorbed by the PET. The modification of the lamp power therefore entails a limited effect on the preform temperature. This effect is strictly related to the preform adopted, as longer preforms would be facing also the lamps of layers D and E. All the other machine configurations led to temperature differences larger than the measurement uncertainty.

As previously evidenced, the main contribution to the measurement uncertainty derives from uncertainty of the preform emissivity. Consequently, to obtain more accurate temperature measurements it is mandatory characterizing each lot of preforms. The maximum emissivity variation observed in a single lot was 0.04; this value suggests that the power of the lamps should be tuned observing at least 3 – 4 samples to obtain an uncertainty lower than 1°C; in this way, it would be possible to clearly distinguish the effects of 5% variation of the lamps power.

Since the measured cooling rate is limited (less than 0.5 °C/s), the use of a moving thermopile can be a good alternative to the IR camera to measure also the temperature distribution of the external surface. In our tests, performed with a non-optimized linear motor, the time duration of a measurement (descent – ascent) was less than 2 s. The cooling during the measurement was therefore comparable to the measurement uncertainty, and the average between descent and ascent (with the same duration) allows a self-compensation of the combined effect of cooling and sensor motion. In any case, the measurement time can be reduced by increasing the speed of the motor or by using an array of detectors; given their time constant, the adoption of fast motors would not lead to noticeable dynamic errors.

6 Conclusions

In this work, we have described a method for the measurement of the internal and external temperature of preforms for ISBM. The method is based on infrared detectors and can be easily implemented on-board ISBM machines during the production phase. The system validation performed on an industrial ISBM machine indicates that the system allows detecting the changes of the temperature profile corresponding to the least significant change in the machine settings. The uncertainty budget proved that the proposed approach allows distinguishing temperature differences of a few degrees (standard uncertainty 1.4°C if the emissivity of the preform lot is measured). This value is satisfying, given that the finer machine tuning performed by the operator usually leads to temperature variations of 2 – 3 °C. The use of a unique emissivity value for all preforms would lead to a standard uncertainty of 4 °C: since the use of a wrong emissivity would lead to a systematic error on the temperatures of the same lot, it would be possible to use the proposed system for temperature control within the same lot. The low cooling rate allowed for the use of a moving sensor with a scan time of about 1 s without significantly increasing the measurement uncertainty.

Acknowledgements

This research was funded by SMIgroup company under an agreement with Dipartimento di Meccanica, Politecnico di Milano.

References:

1. **D.V. Rosato, A.V. Rosato, D.P. Di Mattia.** *Blow Molding Handbook: Technology, Performance, Markets, Economics. The Complete Blow Molding Operation.* Cincinnati : Hanser Gardner, 2004.

2. **A.M. Adams, C.P. Buckley, D.P. Jones.** Biaxial hot drawing of poly(ethylene terephthalate): measurements and modelling of strain-stiffening. *Polymer.* 2000, Vol. 41, pp. 771–786.

3. **M. Bordival, F.M. Schmidt, Y. Le Maoult, V. Velay.** Optimization of Preform Temperature Distribution for the Stretch-Blow Molding of PET Bottles: Infrared Heating and Blowing Modeling. *Polymer Engineering & Science.* 2009, Vol. 49, 4, pp. 783-793.

4. **A.A. Ranjbar, M. Mirsadeghi.** An Inverse Estimation of initial temperature profile in a polymer process. *Polymer Engineering and Science.* 2008, Vol. 48, 1, pp. 133-140.

5. **B. Cosson, F. Schmidt, Y. Le Maoult, M. Bordival.** Infrared heating stage simulation of semi-transparent media (PET) using ray tracing method. *Int J Mater Form.* 2011, Vol. 4, 1, pp. 1-10.

6. **S. Monteix, Y. Le Maoult, F. Schmidt, J.P. Arcens.** Quantitative infrared thermography applied to blow moulding process: measurement of a heat transfer coefficient. *Quantitative InfraRed Thermography Journal.* 2004, Vol. 1, 2, pp. 133-150.

7. *A Stationary System of Noncontact Temperature Measurement and Hotbox Detecting.* **M.Z.Sreckovic, S.D. Milic and.** 5, Sept 2008, Vehicular Technology, IEEE Transactions on, Vol. 57, pp. 2684-2694.

8. *Design of infrared temperature monitoring system applied to the stator of evaporative cooling hydrogenerators.* **Lin, Huang Jing and R.** 2010. Electrical Machines and Systems (ICEMS), 2010 International Conference on. p. 1374-1377.

9. *Implementation of remote temperature-measuring by using a thermopile for Wireless Sensor Network.* **Huang, Chin-Fu Tsai and Wei-Sheng.** 2012. Industrial Electronics and Applications (ICIEA), 2012 7th IEEE Conference on. p. 1325-1328.

10. **X.F. Lux, J.N. Hay.** Isothermal crystallization kinetics and melting behaviour of poly(ethylene terephthalate). *Polymer.* 2001, Vol. 42, 23, pp. 9423-9431.

11. **S. Monteix, F. Schmidt, Y. Le Maoult, R.B. Yedder, R.W. Diraddo, D. Laroche.** Experimental study and numerical simulation of preform or sheet exposed to infrared radiative heating. *Journal of Materials Processing Technology.* 2001, Vol. 119, 1, pp. 90-97.

12. **G.H. Menary, C.W. Tan, C.G. Armstrong, Y. Salomeia, M. Picard, N. Billon.** Validating Injection Stretch-Blow Molding Simulation Through Free Blow Trials. *Polymer engineering and science.* 2010, Vol. 50, 5, pp. 1047-1057.

13. **Demirel, B. e Daver, F.** Experimental Study of Preform Reheat Temperature in Two-Stage Injection Stretch Blow Molding. *POLYMER ENGINEERING AND SCIENCE.* 2013, Vol. 53, 4, p. 868-873.

14. **F. Daver, B. Demirel.** A simulation study of the effect of preform cooling time in injection stretch. *Journal of Materials Processing Technology.* 2012, Vol. 53, 12, pp. 2400-2405.

15. **Kruse, P.W.** *Uncooled thermal imaging: Arrays, Systems and applications.* Bellingham : SPIE press, 2001.

16. *Estimation of the orthosis-limb contact pressure through thermal imaging.* **M. Tarabini, B. Saggin, D. Scaccabarozzi and G. Lanfranchi.** 2012. Instrumentation and Measurement Technology Conference (I2MTC), 2012 IEEE International. pp. 2733-2737.

17. **D. Scaccabarozzi, B. Saggin.** About the dynamic characterization of micro-bolometric infrared cameras. *Sensor and Actuator A.* 2014, Vol. 217, pp. 68-74.

18. **https://www.arduino.cc. [Online]**

19. A. Ruvolo-Filho, G.M. De Carvalho. Correlation between crystallinity, sorption properties, and some infrared bands in the spectra of poly(ethylene terephthalate) films. *J. of Macromolecular Science - Physics.* B, 1996, Vol. 35, 2, pp. 255-264.

20. H. Budzier, G. Gerlach. *Thermal Infrared Sensor: Theory, Optimization and Practice.* Chichester : John Wiley & Sons, 2011.

21. Chung-Nan., C. Temperature Error Analysis and Parameter Extraction of an 8-14 μm Thermopile With a Wavelength-Independent Absorber for Tympanic Thermometer. *IEEE Sensors Journal.* 2011, Vol. 11, 10, pp. 2310-2317.

22. D. York, N.M. Evensen, M.L. Martinez, J. De Basabe Delgado. Unified equations for the slope, intercept, and standard errors of the best straight line. *American Journal of Physics.* 2004, Vols. 72, pp., pp. 367-375.

23. *ISO-GUIDE 98-part 3.* s.l. : ISO, 2008.

24. http://www.smigroup.it. [Online]